Nuclear Engineering and Technology 55 (2023) 3831–3843

Contents lists available at ScienceDirect

Nuclear Engineering and Technology

journal homepage: www.elsevier.com/locate/net

Original Article

Influence of Ca–Na–Cl physicochemical solution properties on the adsorption of Se(-II) onto granite and MX-80 bentonite

Joshua Racette [a, *], Andrew Walker [a], Shinya Nagasaki [a], Tianxiao Tammy Yang [b], Takumi Saito [c], Peter Vilks [d]

[a] Department of Engineering Physics, McMaster University, 1280 Main St. W., Hamilton, Ontario, L8S 4L7, Canada
[b] Nuclear Waste Management Organization, 22 St. Clair Ave. E., Fourth Floor, Toronto, Ontario, M4T 2S3, Canada
[c] Nuclear Professional School, University of Tokyo Hongo Campus, Bunkyo City, Tokyo, 113-8564, Japan
[d] Canadian Nuclear Laboratories Whiteshell Laboratories, 1 Ara Mooradian Way, Pinawa, Manitoba, R0E 1L0, Canada

ARTICLE INFO

Article history:
Received 6 June 2022
Received in revised form
26 June 2023
Accepted 27 June 2023
Available online 28 June 2023

Keywords:
Se(-II)
Adsorption
Surface complexation modelling
Granite
MX-80
Deep geologic repository

ABSTRACT

The adsorption behaviour of Se(-II) onto granite and MX-80 bentonite in Ca–Na–Cl solutions has been studied utilizing adsorption experiments and surface complexation modelling. Adsorption kinetic experiments allude to steady-state adsorption periods after 7 days for granite and 14 days for MX-80 bentonite. Batch adsorption experiments were carried out to determine the influence that the physicochemical solution properties would have on Se(-II) adsorption behaviour. Adsorption of Se(-II) onto granite and MX-80 bentonite follows the trend of anionic adsorption, with a decrease in R_d values as the solution pH increased. There is also an ionic strength influence on the adsorption of Se(-II) onto granite with a decrease in the R_d value as the ionic strength increased. This effect is not found when observing Se(-II) adsorption onto MX-80 bentonite. Final experiments with a representative groundwater, determined that the adsorption of Se(-II) onto granite and MX-80 bentonite returned R_d values of (1.80 ± 0.10) $m^3 \bullet kg^{-1}$ and (0.47 ± 0.38) $m^3 \bullet kg^{-1}$, respectively. In support of the experiments, a surface complexation modelling approach has been employed to simulate the adsorption of Se(-II) onto granite and MX-80 bentonite, where it was determined that two different surface complexes, $\equiv S\_Se^-$ *and* $\equiv SOH_2^+\_H_2Se$ were capable of simulating Se(-II) adsorption behaviour.

1. Introduction

The current methodology to safely dispose of used nuclear fuel in Canada is with the implementation of a Deep Geologic Repository (DGR). Both crystalline and sedimentary rocks are being considered as potential host rock formations for a DGR for used nuclear fuel waste in Canada [1,2]. Brackish to saline groundwaters were observed in crystalline rock at repository depths. For example, the reference groundwater CR-10 representing the potential groundwater chemistry conditions in crystalline rock at repository depths is a Ca-Na-Cl type with a total dissolved solids (TDS) concentration of 11.3 g/L or an ionic strength of 0.24 mol/kgw [3]. In the DGR concept, used nuclear fuel will be packed into used fuel containers which are then entombed within bentonite clay buffer boxes before emplacement within the repository for disposal [1–4]. The combination of a natural geosphere barrier and the engineered barrier are expected to be effective in maintaining hydraulic conditions in the near-field of the repository and ensure that migration of radionuclides is diffusion controlled. If a radionuclide release event occurs, it is expected that both the engineered and geosphere barriers will retard the diffusivity of radionuclides. Both adsorption experiments and surface complexation modelling allow for an improved understanding of this adsorption behaviour.

Presently, the NWMO have identified ^{79}Se to be one of the potentially significant radionuclides that exist within used nuclear fuel as it is a concern from a radiological and chemical standpoint [3]. The radiological concern associated with ^{79}Se is attributed to the long half-life of 3.27×10^5 years, the sole β^- decay process where the emitted radiation has a maximum energy of $E_{max} = 150.9$ keV and the decay product is ^{79}Br, and lastly there is an associated 0.6% instant release fraction [5–10]. The amount of ^{79}Se

* Corresponding author.
E-mail addresses: racettjj@mcmaster.ca (J. Racette), walkerat@mcmaster.ca (A. Walker), nagasas@mcmaster.ca (S. Nagasaki), tyang@nwmo.ca (T.T. Yang), saito@n.t.u-tokyo.ac.jp (T. Saito), peter.vilks@cnl.ca (P. Vilks).

https://doi.org/10.1016/j.net.2023.06.049

that is found within used nuclear fuel is dependent upon the burnup of the fuel when removed from the reactor. It is currently reported that for CANDU nuclear fuel with a burnup of 220 MWh•kgU^{-1}, the ^{79}Se inventory is 1.76 × 10^{-5} mol•kgU^{-1}. Whereas with a burnup of 280 MWh•kgU^{-1}, the ^{79}Se inventory increases to 2.20 × 10^{-5} mol•kgU^{-1} [3]. In addition to the radiological hazard, the chemical behaviour of ^{79}Se will allow it to be up taken by the biosphere with ease [11–17].

Selenium exhibits redox sensitive behaviour which compounds the necessity associated with understanding migration processes associated with unique selenium species. When aerobic and oxidizing conditions are present, Se will exist as either Se(VI) or Se(IV) which chemically speciate as selenate, SeO_4^{2-} and selenite, SeO_3^{2-}, respectively. When Se is under these anerobic, reducing, and neutral pH conditions the dominant valence state is Se(-II), which chemically speciates as the anion hydroselenide, HSe^-. In the past, there has been an abundant number of studies performed that explored the adsorption behaviour of both Se(VI) and Se(IV) [18–38]. This is starkly contrasted by the few studies pertaining to Se(-II) adsorption [39–44]. To the authors' present knowledge there is no published material specific to Se(-II) adsorption onto Canadian crystalline rocks under both saline and reducing conditions.

The adsorption behaviour of Se(-II) onto granite and MX-80 bentonite has been elucidated as a function of Ca–Na–Cl physicochemical solution properties which include the solutions pH and ionic strength. For reference the units associated with ionic strength of all solutions are reported in molality [mol•kgw^{-1} (mol•(kilogram water)$^{-1}$)], and not molarity [mol•L^{-1}]. Ionic strengths that were experimentally investigated are 0.05, 0.1, 0.24, and 1.0 mol•kgw^{-1}. pH values tested are 5.0, 6.0, 8.0, and 9.0. An additional experiment was performed to determine the adsorption of Se(-II) onto granite and MX-80 bentonite in CR-10 solution. Furthermore, non-electrostatic surface complexation models are presented which have been optimized using batch adsorption experiment results.

2. Materials and experimental methodology

All chemicals in the experiments were reagent grade and supplied by Fisher Scientific unless explicitly stated. Solid masses of chemicals and adsorbent materials were measured using a Sartorius Quintix 213-1S scale. Deionized water was prepared using a Milli-Q Direct 8 system which guarantees that the volumetric resistivity of the deionized water is 18.2 MΩ cm. To ensure anoxic conditions were present for the duration of the experiments, a precise controlled atmospheric glovebox supplied by Labconco was utilized. This glovebox was filled with N_2 gas (>99.999%), which was constantly flowing through the glovebox for the duration of the experiments to continuously vent the glovebox, preserving O_2 levels below 2.0 ppm and to ensure that contaminant CO_2 is removed. Reducing conditions are introduced when hydrazine monohydrate ($N_2H_4 \cdot H_2O$) is utilized within the Se reduction methodology. A Fisherbrand accumet AB200 Benchtop pH meter was used in conjunction with a Fisherbrand accumet pH combination electrode (#13-620-297), and a platinum tipped Fisherbrand accumet Metallic ORP electrode (#13-620-115) to determine the pH and Eh, respectively. Calibration of the pH meter was completed using pH 4.0, 7.0, and 10.0 pH buffer solutions. Fig. S1 in the Supplementary Material presents a Se Pourbaix diagram with the results of all Eh vs. pH_m measurements [45]. To coincide with the Pourbaix diagram, all Eh (vs. SHE) values were converted to pe. An important topic to discuss is that the adsorption kinetic and batch adsorption experiments investigate ionic strengths greater than 0.1 mol•kgw^{-1}. This requires that the measured pH value (pH_{obs}) be designated as an operational apparent value. Any one pH_{obs} value is related to a molal H^+ concentration (pH_m = -log m_{H+}), and a molar H^+ concentration (pH_c = -log c_{H+}), through a linear relationship of the form $pH_{m,\,c} = pH_{obs} + A_{m,\,c}$. Where $A_{m,\,c}$ is an empirical correction factor that accounts for variation in liquid junction potential between measuring in dilute and saline solutions, and the individual H^+ activity coefficient [46–48]. This study used the molal pH_m conversion opposed to the molar pH_c conversions. Linear relationships were derived for all Ca–Na–Cl solutions with a Metrohm Ti-Touch 916. Table 1 presents the $pH_m = pH_{obs} + A_m$ conversion relationships for the 0.05, 0.1, 0.24, and 1.0 mol•kgw^{-1} Ca–Na–Cl solutions.

The reduction of Se was completed using a chemical reduction methodology which has been proven to be adequate in reducing either Se(VI) and Se(IV) to Se(-II) [40–43,49–54]. All Se used in adsorption kinetic and batch adsorption experiments is derived from a 1000 ± 1 μg mL^{-1} standard solution within a 1.0% nitric acid matrix that was supplied by Agilent Technologies. No confirmation of the exact Se redox state in the standard solution was completed and as such, the standard solution was presumed to contain a mixture of both Se(IV) and Se(VI). Preparation of all Se solutions and the subsequent storage of these solutions was performed within the glovebox. This was to ensure that anoxic conditions were preserved during the reduction process, and throughout the duration of all experiments. An aliquot of the standard solution was mixed with deionized water so that the resultant Se concentration was 1.0 μmol L^{-1}. Preliminary experiments were performed to ensure this concentration was below the solubility of Se(cr). Then an amount of 0.2 mol L^{-1} hydrazine monohydrate was added to the Se solution to ensure reducing conditions were present. Finally, the Se solution was allowed to mature for a minimum of five days to ensure Se(-II) was the dominant oxidation state within the Se solution. Preliminary stability experiments were performed which measured the concentration of the reduced Se(-II) for more than a month. There was no change in concentration during the month, and as such this was considered evidence for the success in the reduction methodology regarding the stability of Se(-II). This ensures that Se(-II) will be the predominant redox state for the duration of all adsorption experiments. The absorbance spectrum was measured over the course of a month and was found to be unchanged, this provided further confidence that Se(-II) is stable in solution. The UV-VIS spectrum measured after reduction of Se to Se(-II) did not show an appreciable peak which could be attributed to HSe^-. However, with consideration that the concentration of Se(-II) in solution is 1.00 μmol L^{-1} and the solution pH is in the neutral pH regime of pH = 6.4, a predominant absorbance spectrum may not be discernible. A comment regarding Se(-II) spectra, is that it becomes more prominent as the concentration of Se in solution increases, and as the solution pH increases towards a more basic pH value [40–42,51–54]. Therefore, it is considered plausible presently, that no discernible peak may be visible despite the reduction methodology being successful. Previously, Iida et al., remarked that absorption spectra peaks were assigned to Se(-II) species from solubility experiments in the undersaturation direction, but not the oversaturation direction due to a Se(-II) concentration that was

Table 1
$pH_m = pH_{obs} + A_m$ conversion relationships for Ca–Na–Cl solutions with ionic strengths of 0.05, 0.1, 0.24, and 1.0 mol•kgw^{-1}.

Ionic Strength [mol•kgw^{-1}]	$pH_m = pH_{obs} + A_m$ conversion relationships
0.05	$pH_m = 1.0570 \bullet pH_{obs} - 0.2838$
0.10	$pH_m = 1.0470 \bullet pH_{obs} - 0.2682$
0.24	$pH_m = 1.0507 \bullet pH_{obs} - 0.1593$
1.00	$pH_m = 1.0671 \bullet pH_{obs} - 0.0227$

considered too low [53]. Iida et al., reported that the concentration of Se(-II) from oversaturation experiments is approximately on par with the concentration of Se(-II) used in this study [53]. Further, Iida et al. reported that the pH of the solution in oversaturation experiments are of similar circumneutral pH values as to the pH = 6.4 of the measured solution in this study, this is considered as justification for the lack of an observable spectra peak [53]. Undersaturation experiments carried out by Iida et al. did return an observable Se(-II) spectra at 247.0 nm which was assigned to HSe^- [53]. The concentration of Se(-II) in the undersaturation experiments were on the order of 10.0–100.0 μmol L^{-1} with solution pH values greater than 9.0 [53]. Previously, Walker et al., included the UV-VIS spectrum in their study which focused on Se(-II) adsorption in Na–Ca–Cl solutions [43]. The reduction methodology utilized by Walker et al., with success is identical to the reduction methodology utilized within this study, providing confidence that this methodology is successful in Ca–Na–Cl solutions [43].

The CR-10 reference saline groundwater solution has a known pH of 7, an Eh of −200 mV (vs. SHE), and a total dissolved solids content of 11.3 g L^{-1} [3]. Table 2 presents the mass of compounds required to produce CR-10 and are presented in order of addition to properly prepare the CR-10 solution [55]. Additionally, to ensure reducing conditions were present there will be 0.2 mol L^{-1} hydrazine monohydrate added to the prepared 1.0 L CR-10 solution. A reminder is that the hydrazine monohydrate will act as a chemical buffer and increase the pH of the CR-10 solution. This required the addition of 0.1 N HCl to adjust the pH back to the required pH_m initial value.

Four different Ca–Na–Cl solutions were prepared with ionic strengths of 0.05, 0.1, 0.24, and 1.0 mol•kgw^{-1}. All four solutions have a constant Na/Ca ratio of 1.60 which is approximately the same Na/Ca ratio as the CR-10 solution. Table 3 presents masses required of the NaCl and $CaCl_2 \cdot 2H_2O$ salts used to prepare the Ca–Na–Cl solutions. Then to ensure reducing conditions are present, 0.2 mol L^{-1} hydrazine monohydrate is added to the Ca–Na–Cl solutions. Subsequently, the pH of the solutions are then adjusted to the required pH_m value using 0.1 N HCl.

Granite has been supplied by the NWMO and originates from the Lac du Bonnet batholith in Manitoba, Canada. The granite was crushed with a tungsten carbide cylinder supplied by Nichika. Then with a range of stainless-steel sieves, particles that varied in size between 150.0 μm and 300.0 μm were collected and used in subsequent adsorption experiments. The MX-80 bentonite clay was supplied by the American Colloid Company after being sourced from Wyoming, USA. MX-80 bentonite was used as received throughout all adsorption experiments. Table 4 presents an average mineralogical breakdown for granite and MX-80 that was determined from a petrographic analysis of granite supplied by the NWMO, and an averaging of XRD data specific to MX-80 bentonite clay [56–58].

Table 2
Masses required, and molal concentration of all compounds used to prepare 1.0 L CR-10 saline solution. Error on all masses is ±0.0001 g. Ionic strength of CR-10 is approximately 0.24 mol•kgw^{-1} for reference.

Compound	Mass [g]	Molal Concentration [mol•kgw^{-1}]
NaCl	4.830	0.0823
KCl	0.029	0.0004
$CaCl_2 \cdot 2H_2O$	6.280	0.0429
$MgCl_2 \cdot 6H_2O$	0.502	0.0025
$SrCl_2 \cdot 6H_2O$	0.076	0.0003
$CaSO_4 \cdot 2H_2O$	1.610	0.0094
$NaHCO_3$	0.087	0.0010

Table 3
Masses required of NaCl and $CaCl_2 \cdot 2H_2O$ salts respectively that were used to prepare 1.0 L of 0.05, 0.1, 0.24, or 1.0 mol•kgw^{-1} Ca–Na–Cl solutions. Error on all masses is ±0.0001 g.

Ionic Strength	NaCl Mass [g]	$CaCl_2 \cdot 2H_2O$ Mass [g]
0.05	1.019	1.598
0.10	2.038	3.196
0.24	4.891	7.670
1.00	20.38	31.96

3. Adsorption experiments

Prior to initiation of the adsorption experiments, the granite and MX-80 bentonite samples were preconditioned. Preconditioning was completed using either the CR-10 solution, or one of the Ca–Na–Cl solutions. The pH_m of each sample being preconditioned was also adjusted, if needed to a pH_m of 7.0 for the CR-10 solution, or a pH_m of 5.0, 6.0, 8.0, or 9.0 for the Ca–Na–Cl solutions. Each sample being preconditioned contains (20.0 ± 1.0) mg of the solid adsorbent and (5.0 ± 0.05) mL of precondition solution. Samples were agitated daily to ensure preconditioning was effective. Upon completion of the preconditioning period, the samples were centrifuged for 6.0 min at 5860.0 RPM or approximately 3000.0 RCF using a Beckman Coulter Allegra X–30R benchtop centrifuge equipped with a F0630 rotor to separate the liquid and solid components. Centrifugation of these samples was limited by the rotational velocity that the polycarbonate reaction vessel can withstand before being compromised. Finally, within the glovebox, the precondition solution was removed using a pipette to minimize any potential agitation of the centrifuged solids. Adsorption kinetic and batch adsorption experiments then begin upon addition of CR-10 or one of the Ca–Na–Cl solutions that had been spiked with Se(-II).

All adsorption experiments have been performed in triplicate, at room temperature, inside of the N_2 atmospheric glovebox. A preliminary experiment was performed and determined that adsorption of Se(-II) onto the walls of the polycarbonate reaction vessel was negligible. The initial concentration of Se(-II) used in all experiments was on average (1.00 ± 0.5) μmol•L^{-1} which is below the expected solubility limit of Se(-II) ensuring that no Se precipitate should form within solution during the experiments. The adsorption of Se(-II) onto either of the adsorbents was quantified with the adsorption distribution ratio R_d [m^3•kg^{-1}], and is calculated following Equation (1). Where: $C_{initial}$ is the initial Se(-II) concentration in solution [mol], C_{final} is the final Se(-II) concentration remaining in solution [mol], L is the volumetric liquid amount [m^3], and M is the solid adsorbent mass [kg].

$$R_d = \frac{C_{initial} - C_{final}}{C_{final}} \bullet \frac{L}{M} \quad (1)$$

Table 4
Average mineralogical composition of granite and MX-80 bentonite.

Mineral Assemblage	Granite [wt %]	MX-80 bentonite[b] [wt %]
Quartz	34.0	3.62
Albite	0.00	3.54
Biotite	3.00	0.00
Montmorillonite	0.00	85.4
Plagioclase Feldspar	37.0	0.00
Alkali Feldspar	19.0	0.00
Others	6.60[a]	0.00

[a] The assemblage components chlorite, hornblende, epidote, muscovite, sphene, zircon, and myrmekite contribute ~1.0% each.
[b] The total mineral assemblage amount for MX-80 bentonite sums to 92.56%. The remaining 7.44% is attributed to the presence of amorphous solids.

Both adsorption kinetic and batch adsorption experiments utilized an identical methodology to quantify the concentration of Se(-II) remaining in solution. A 5.00 mL aliquot was removed from each reaction vessel and placed into a Nalgene Oakridge centrifuge container and centrifuged at 18000.0 RPM or 27579.0 RCF for 30.0 min with the Beckman Coulter X–30R centrifuge that was now equipped with a F1010 rotor. A previous NWMO technical report confirms that this is adequate centrifugation to separate the liquid and solid components [59]. Subsequently, a 0.5 mL aliquot of the supernatant solution was removed and mixed with 9.5 mL of deionized water and then measured using an Agilent 8800 Inductively Coupled Mass Spectrometer (ICP-MS). This dilution is required as the solution salinity is required to be below 0.75 mol L^{-1} for accurate measurement with the ICP-MS [43,60].

Initially, it was important to determine the Se(-II) adsorption kinetic steady-state period for both adsorbents. In all experiments, there was the (20.0 ± 1.0) mg of preconditioned adsorbent with (10.0 ± 0.5) mL of liquid for a resultant liquid/solid ratio of (0.50 ± 0.03) $m^3 \bullet kg^{-1}$. Two ionic strength solutions, which correspond with the maximum and minimum Ca–Na–Cl ionic strengths of 0.05 and 1.0 mol•kgw^{-1} were used for adsorption kinetic experiments. Concentrations of Se(-II) were measured after *1, 2, 4, 8, 10, 15,* and *20* days for granite, and after *1, 2, 4, 8, 10, 16,* and *20* days for MX-80 bentonite. For the duration of adsorption kinetic experiments, the pH_m and Eh were measured at each time interval to confirm that redox conditions were present within the polycarbonate reaction vessel, to ensure that no oxidation of Se(-II) may have taken place.

After the adsorption kinetic steady-state period was determined, batch adsorption experiments were performed. Ionic strength dependency experiments were measured at 0.05, 0.1, 0.24, and 1.0 mol•kgw^{-1}. pH_m dependency experiments were measured at pH_m values of 5.0, 6.0, 8.0, and 9.0. Concurrently a batch adsorption experiment was carried out with the CR-10 solution and the same adsorption kinetic steady-state period was used as in the physicochemical solution property dependency experiments. The pH_m of the CR-10 solution was adjusted to a pH_m value of 7.0. Throughout all batch adsorption experiments, pH_m and Eh measurements were recorded daily to confirm reducing conditions were maintained preventing the oxidation of Se(-II). If the measured pH_m value differed from the required pH_m value by more than 0.2 units adjustment was performed through addition of either 0.1 N HCl or 0.1 N NaOH.

4. Surface complexation modelling

The Ca–Na–Cl physicochemical solution property dependency adsorption experiments with granite and MX-80 bentonite have been simulated using a surface complexation model with the geochemical code PHREEQC [61]. It is important to recall that when modelling in solutions that have substantial ionic strengths, a proper method must be invoked to account for increased electrostatic interactions between ions of specific interest, and the background electrolyte ions. Specific Ion Interaction theory was employed to calculate activity coefficients following Equation (2) [45]. Where: z_j is the charge of ion *j*, *D* is the Debye-Hückel term, m_k is the molality of ion *k,* which is oppositely charged to ion *j*, and $\epsilon(j, k)$ is the specific ion interaction parameter.

$$\log\left(\gamma_j\right) = -z_j^2 D + \sum_k \epsilon(j,k) m_k \quad (2)$$

Relevant SIT parameters used throughout the modelling are presented in Table 5. All solutions being modelled have an identical Na/Ca ratio, ionic strength, and Ca–Na–Cl concentrations as the solutions used in experiments. All simulations have a Se(-II) concentration of 1.00 μmol•kgw^{-1}, which is on par with the initial Se(-II) concentration used throughout the experiments. Thermodynamic information specific to Se(-II) is found in both the Nuclear Energy Agency's and Japanese Atomic Energy Agency's thermodynamic databases [45,62]. No polyselenide species of the form Se_n^{2-} where $n = 1–4$, were included in the modelling as it was assumed that these species would form only in more alkaline conditions where $pH_m \geq 10$ [63,64]. To establish a surface complexation model that best simulates the adsorption of Se(-II), both surface complexation and ion exchange reactions should be considered. Given that adsorption of an anion was being simulated, ion exchange reactions are not important as they are specific to cations. Therefore, the formation of Se(-II) surface complexes is one possible mechanism to model the adsorption of Se(-II).

The model that is used to describe a single mineral assemblage surface is a 2-site non-electrostatic surface complexation (2SPNE SC) model. Previously, 2SPNE SC models have been shown to be capable of simulating adsorption of various radionuclides onto different materials with success [43,59,66–72]. In the 2SPNE SC model, the surface is comprised of amphoteric surface sites which are analogous to the surface functional groups found at the edges of aluminosilicate minerals. As this is a 2-site model, there are both strong and weak sites to be considered respectively. However, with modelling of Se(-II) adsorption being performed at trace concentrations, only the strong sites found within the 2SPNE SC model need to be considered [43,59,66–72]. These surface sites are amphoteric in nature as mentioned and are assumed to protonate and deprotonate with respect to the background solution pH. This protonation behaviour would lead to the formation of an electric double layer which provides a variable surface charge for the simulated surface.

To properly simulate the adsorption of Se(-II) onto both granite and MX-80 bentonite, a component additive surface complexation model approach has been used. From Table 4 it is apparent that both adsorbents are comprised of numerous homogenous mineral assemblage components, where each mineral assemblage has its own unique protolysis characteristics, and surface properties. It is believed that a heterogenous surface comprised of multiple surfaces will provide more flexibility to model across the pH range as the different surfaces will exhibit different protolysis behaviours. A model assumption is that the specific surface area (SSA) associated with a heterogenous adsorbent surface being simulated is distributed proportionately across the assemblage components. Therefore, the SSA's for each mineral assemblage have been calculated following (3). Where $SSA_{adsorbent}$ is the SSA of the mineral being simulated. For reference, $SSA_{granite} = 0.18\ m^2\ g^{-1}$ and $SSA_{MX\text{-}80\ bentonite} = 8.5\ m^2\ g^{-1}$ [39,73]. SSA for granite was determined with N_2 Brünauer-Emmett-Teller (BET) measurements [39]. SSA for MX-80 bentonite was determined from Atomic Force Microscopy (AFM) and low-pressure gas adsorption experiments. An important comment is this MX-80 bentonite surface utilizes the lateral edge SSA of 8.5 $m^2\ g^{-1}$, as opposed to larger SSA's of 26.6 $m^2\ g^{-1}$, 753.0 $m^2\ g^{-1}$, or 788.0 $m^2\ g^{-1}$, which are attributed to the basal plane, interlayer, and total SSA of MX-80 bentonite, respectively [73]. This is considered to improve the MX-80 bentonite model by restricting the maximum number of possible adsorption sites on the surface which is believed to assist in preventing either an under- or overprediction of the concentration of any modelled surface complex. This should provide more appropriate surface complexation constants for the presumed surface complexation reactions within the given MX-80 bentonite model. Site densities for mineral assemblages are used directly in the model as reported. Another assumption for this model is that the site density of a mineral assemblage within a heterogenous mineral must equal the site

Table 5
Selected ion interaction coefficients and the different reactions specific to Se(-II) utilized throughout the surface complexation modelling.

Ion Interaction Coefficients				
Cation (ion j)	Anion (ion k)	ε(j, k) [kg•mol^{-1}]	Error	Reference
Na^+	OH^-	0.04	0.01	[62]
Na^+	Cl^-	0.03	0.01	[45]
Ca^{2+}	Cl^-	0.15	0.01	[45]
H^+	Cl^-	0.12	0.01	[62]
Na^+	HSe^-	- 0.01	0.10	[45]
Ca^{2+}	HSe^-	0.15[a]	0.01	[This study]
Se(-II) Reactions				
Reaction		Log K	Error	Reference
$HSe^- + H^+ \leftrightarrow H_2Se(aq)$		3.850	0.050	[62]
$H^+ + SeO_4^{2-} \leftrightarrow HSeO_4^-$		1.750	0.100	[62]
$2H^+ + SeO_3^{2-} \leftrightarrow H_2SeO_3(aq)$		11.00	0.269	[62]
$H^+ + SeO_3^{2-} \leftrightarrow HSeO_3^-$		8.360	0.230	[62]
$SeO_4^{2-} + 9H^+ - 4H_2O + 8\ e^- \leftrightarrow HSe^-$		81.75	0.435	[62]
$SeO_4^{2-} + 2H^+ + 2\ e^- - H_2O \leftrightarrow SeO_3^{2-}$		28.04	0.397	[62]

[a] $\varepsilon(Ca^{2+}, HSe^-)$ ion interaction coefficient is an estimation based upon corresponding charge type $\varepsilon(Ca^{2+}, X^-) = 0.15$ kg mol^{-1} [65].

density of the assemblage mineral if found in a homogenous form.

$$SSA_i = SSA_{adsorbent} \bullet (Mass\ Fraction\ of\ Mineral\ Assemblage)_i \quad (3)$$

It has been reported that there are two possible Se(-II) surface complexes with mineral surfaces which are described with (4) and (5) [40,43]. The first surface complexation reaction is assumed to be a chemically specific interaction between the HSe^- anion and the surface hydroxyl groups. In contrast, the second surface complexation reaction is assumed to be non-specific, and similar surface complexes would form with background electrolytes and the simulated surface [74].

$$\equiv SOH + HSe^- \leftrightarrow \equiv SSe^- + H_2O \quad (4)$$

$$\equiv SOH + HSe^- \leftrightarrow \equiv SOH_2HSe \quad (5a)$$

Granite has been assumed to be 56.0% K-feldspar, 34.0% quartz, and 3.0% biotite. MX-80 bentonite has been assumed to be 85.4% montmorillonite, 3.62% quartz, and 3.54% albite. Protolysis constants for each mineral assemblage are presented in Table 6. To support utilizing this component additive surface complexation modelling approach, there has been proven success in simulated adsorption onto a granite sample from Inada, Japan [75]. This previous model used an albite surface as one of the assemblage surfaces to describe a proportion of granite. To simplify the modelling of both granite and MX-80 bentonite the protolysis constants and site density that was used to define albite in the previously presented model have been used to define both the feldspar surface within the granite model, as well as the albite surface within the MX-80 model. A second assumption about the granite model being presented is that the 56.0% feldspar assemblage surface is a summation of the known 37.0% plagioclase feldspar and 19.0% alkali feldspar mineral amount in granite. These assumptions are both made on the basis that albite is a known plagioclase feldspar, and that plagioclase is feldspathic mineral. It should be acknowledged that there may be discrepancies between the surface charge behaviour of albite compared to feldspar as their chemical formulas are $NaAl_3O_8$ and KAl_3O_8, respectively. As this is a non-electrostatic model, the interactions that may occur between the background electrolyte ions and the surface sites are not modelled, and the assumption was presumed justified. Simulated surface descriptions for granite and MX-80 bentonite are presented in Table 7.

5. Results and discussion

Adsorption kinetics for Se(-II) onto the surface of granite and MX-80 bentonite are presented in Fig. 1 and it appears that granite reached adsorption steady state conditions within 3–5 days while MX-80 bentonite reaches adsorption steady-state conditions within 7–10 days. From these adsorption kinetics results, the adsorption steady state period for granite and MX-80 bentonite have been set to 7 and 14 days, respectively. Initial pH_m, final pH_m, and the measured R_d values from the adsorption kinetic experiments are presented in Table 8.

Previously, Iida et al. found that an adsorption kinetic steady-state period of 14 days was required for the adsorption of Se(-II) onto minerals that contain iron such as biotite, geothite, and magnetite [40]. Even though granite is presumed to be 3.0% biotite, a longer adsorption kinetic steady-state period of 14 days compared to 7 days for granite may be in part to the quartz component which does not exhibit any predilection for Se(-II) adsorption [40]. With this difference in the iron-containing minerals within granite, and the possibility that adsorption reactions which involve Se(-II) and iron may require more time to reach steady-state conditions; as there are possible secondary redox processes which may because for the difference in adsorption kinetic steady-state periods [42]. In addition to determining steady-state periods for iron containing minerals, Iida et al., utilized a 14-day adsorption kinetic steady state period for experiments that involved sandy mudstone and tuffaceous sandstone which coincides with the 14-day period found for Se(-II) adsorption onto MX-80 bentonite [40]. Recently, a study by Sugiura et al., found that a 7-day steady-state period was acceptable for montmorillonite [42]. A point should be made that although MX-80 bentonite is assumed to be 85.4% montmorillonite, the remaining 14.6% may have a slower reaction period with Se(-II), or there may be no interaction expected. When considering the composition of MX-80 bentonite, and recognizing the different possible minerals which may exhibit different Se(-II) adsorption mechanisms, a 14-day kinetics period for MX-80 is believed to be justified. This 14-day adsorption kinetic period has been shown to occur with Se(-II) in Na–Ca–Cl solutions thus providing further justification [43]. In both the 0.05 and 1.00 mol•kgw^{-1} Ca–Na–Cl solutions the adsorption of Se(-II) onto MX-80 bentonite is greater than Se(-II) adsorption onto granite. Similar results have been presented that shows montmorillonite has more capacity to adsorb compared to granite which supports the evidence that MX-80 adsorbs more Se(-II) than granite [42].

Table 6
Protolysis constants for each mineral assemblage considered within the component additive surface complexation model.

Mineral Assemblage Components		Protonation/Deprotonation Reactions		Reference
		$\equiv SOH + H^+ \leftrightarrow \equiv SOH_2^+$	$\equiv SOH \leftrightarrow \equiv SO^- + H^+$	
Protolysis Constants *(Log K)*	Feldspar/Albite	4.13	−8.46	[75]
	Quartz	−1.26	−7.28	[75]
	Biotite	4.60	−6.40	[75]
	Montmorillonite	4.50	−7.90	[66–71]

Table 7
Simulated surfaces and their constituent surfaces with calculated SSA and site densities.

Simulated Surface	Constituent Surface	SSA [$m^2 \bullet g^{-1}$]	Site Density [$sites \bullet nm^{-2}$]	Reference
Granite	Feldspar_sOH	0.1008	4.05	[75]
	Quartz_sOH	0.0612	5.67	[75]
	Biotite_sOH	0.0054	3.81	[75]
MX-80 Bentonite	Montmorillonite_sOH	7.259	5.70	[76]
	Quartz_sOH	0.3077	5.67	[75]
	Albite_sOH	0.3009	4.05	[75]

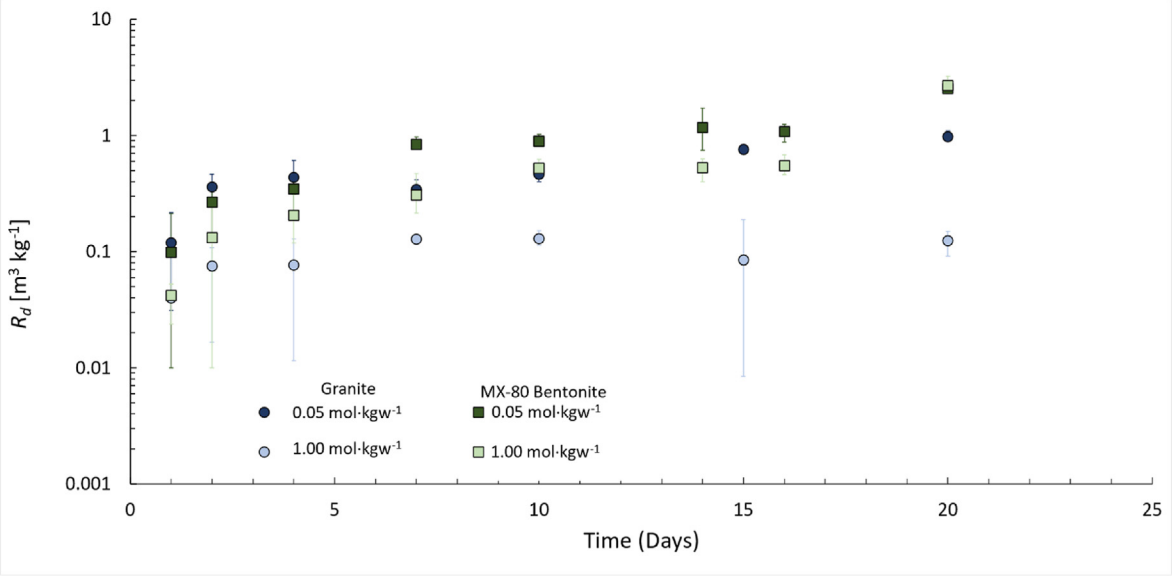

Fig. 1. Adsorption kinetics for Se(-II) onto granite and MX-80 bentonite in 0.05 and 1.0 $mol \bullet kgw^{-1}$ Ca–Na–Cl solutions.

Table 8
Adsorption kinetic initial pH_m, final pH_m, and measured R_d values for granite and MX-80 bentonite in 0.05 and 1.0 $mol \bullet kgw^{-1}$ Ca–Na–Cl solutions.

Adsorbent	Ionic Strength [$mol \bullet kgw^{-1}$]	Initial pH_m	Final pH_m	R_d [$m^3 \bullet kg^{-1}$]
Granite	0.05	9.09 ± 0.2	9.11 ± 0.2	0.76 ± 0.08
	1.00	9.34 ± 0.2	9.38 ± 0.2	0.09 ± 0.01
MX-80 bentonite	0.05	9.10 ± 0.2	9.08 ± 0.2	1.09 ± 0.22
	1.00	9.43 ± 0.2	9.43 ± 0.2	0.55 ± 0.13

A careful observation about the time required for Se(-II) absorption onto granite to reach steady state conditions should be mentioned. From the results presented in Fig. 1, it is possible to discern within error, that steady state conditions are reached within 3–5 days. This is a shorter period than the 7 days that are being utilized in subsequent batch adsorption experiments specific to granite. It is believed that the fast approach to steady state conditions for Se(-II) adsorption onto granite is attributed to rapid surface adsorption processes which dominate Se(-II) adsorption onto granite. This adsorption process is presumed to be described by the non-specific surface complex, $\equiv SOH_2HSe$. However, with the abundance of mineral assemblage components that exist within granite, there is still the assumption that a specific adsorption process is possible, which is described with the $\equiv SSe^-$ surface complex. Given the slower adsorption kinetics associated with specific complexes as opposed to non-specific ones, the increased adsorption kinetic state period of 7 days for granite is considered justified.

Results from batch adsorption experiments that investigate the influence of Ca–Na–Cl physicochemical solution properties on the

Se(-II) adsorption behaviour onto granite and MX-80 bentonite are presented in Figs. 2 and 3, respectively. Surface complexation models that simulate the adsorption of Se(-II) onto granite and MX-80 bentonite are presented in Figs. 2 and 3, respectively. Surface complexation reactions and the associated surface complexation constants are presented in Table 9. Hypothesized surface complexation reactions onto the granite or MX-80 bentonite surfaces are presented in Figs. 4 and 5, respectively.

Adsorption of Se(-II) onto granite displays a typical anionic adsorption trend, with the R_d value decreasing as the solution pH_m increases [39–44]. There is a decrease in the amount of Se(-II) that adsorbs onto the granite surface when $pH_m \geq 8.0$ which is being attributed to the variable surface charge. As Se(-II) exists in solution as HSe^-, there will be Coulombic attractive forces in the acidic regime and repulsive forces in the basic regime. As a result of the repulsive forces expected from the adsorbent surface, the decrease in Se(-II) adsorption at high pH_m values is justified. Additionally, in the Se(-II) – granite system there is an apparent effect that is attributed to the concentration of background electrolytes in solution. This ionic strength effect is noticeable when $pH_m \geq 6.0$ and ionic strength >0.1 mol·kgw^{-1}, these conditions are conducive to observing that the R_d value decreases with an increase in the ionic strength. It is expected that with an increase in the ionic strength there will be an increased amount of background electrolytes which may interact with the HSe^- ion, or the surface itself. It is possible that free Na^+ or Ca^{2+} ions will possibly create Na–Se(-II) or Ca^{2+}-Se(-II) ion pairs. Furthermore, it is presumed that as there is an increase in these background electrolytes, so must the probability of interaction increase between Se(-II) and any one of the free Na^+ or Ca^{2+} ions. With formation of ion pairs, the amount of HSe^- freely available in the solution that can adsorb onto the granite surface will decrease and as such it is expected that R_d would decrease as the ionic strength increases, as observed in Fig. 2. It must also be considered that as ionic strength increases, the amount of free adsorption sites decreases as the Na^+ and Ca^{2+} ions adsorb to the deprotonated surface. This unique effect on the adsorption behaviour has been shown previously with Ni(II) adsorption onto kaolinite [77]. It was argued that with the increase in ionic strength the amount of available adsorption sites must decrease, which must decrease the amount of Ni(II) able to be adsorbed. A second argument also presented is the production of Ni(II)–Cl^- ion pairs which may not interact with the surface. The increase in ionic strength would lead to the increased ion pair formation which is considered to prevent free ions from adsorbing onto the surface through a buffer effect. A final statement is that when $pH_m \leq 5.0$, it is difficult to discern this ionic strength effect on the adsorption of Se(-II). It is presumed that in the acidic regime the large number of protonated surface sites would lead to such a large degree of electrostatic attraction between the HSe^- anion and the positively charged surface. So much so, that any ionic strength effects may be negligible in comparison. Ticknor et al., previously found a similar decrease in adsorption of Se(IV)/Se(VI) onto granite with an increase in ionic strength [39]. Additionally, Ticknor et al., determined that Se(IV)/Se(VI) R_d values with granite were either negligible or had values ranging between 0.00018 and 0.0089 m^3 kg^{-1} [39,78]. With consideration that Se(-II), Se(IV), and Se(VI) all primarily speciate as anions, the similar adsorption behaviour is expected. In a previous study that focused on Se(-II) adsorption onto geothite, magnetite, ferrous oxide, and biotite, the published R_d values were found to range from approximately 0.54 to 38.0 m^3 kg^{-1}, 0.012–0.056 m^3 kg^{-1}, 0.33–1.1 m^3 kg^{-1}, and 0.028–0.13 m^3 kg^{-1} [40]. These R_d values have been reported within the pH range of approximately $7.0 < pH < 9.0$ to more appropriately coincide with the pH_m range utilized within this study [40]. Observation of the R_d values determined through this study, and presented in Fig. 2 between the pH_m regime of 7.0–9.0 are on par with this previous study. There did not appear to be any ionic strength dependant effects present that impacted Se(-II) adsorption onto geothite, magnetite, ferrous oxide, or biotite [40]. Yet, granite does display an ionic strength dependency which may be attributed to any of the mineral assemblage components within granite that is not an iron containing mineral. These previously presented Se(-II) adsorption studies which exhibit similar R_d values and similar adsorption trends with respect to the physicochemical solution properties support the results determined from these Se(-II) adsorption onto granite experiments in Ca–Na–Cl solutions.

Adsorption of Se(-II) onto MX-80 bentonite exhibits a similar trend with respect to solution pH_m as determined from the Se(-II) batch adsorption experiments using granite which is a known anionic adsorption trend [39–44]. At the present, the previous arguments that explained the decrease in Se(-II) adsorption with an increase in solution pH_m when granite was the adsorbent surface

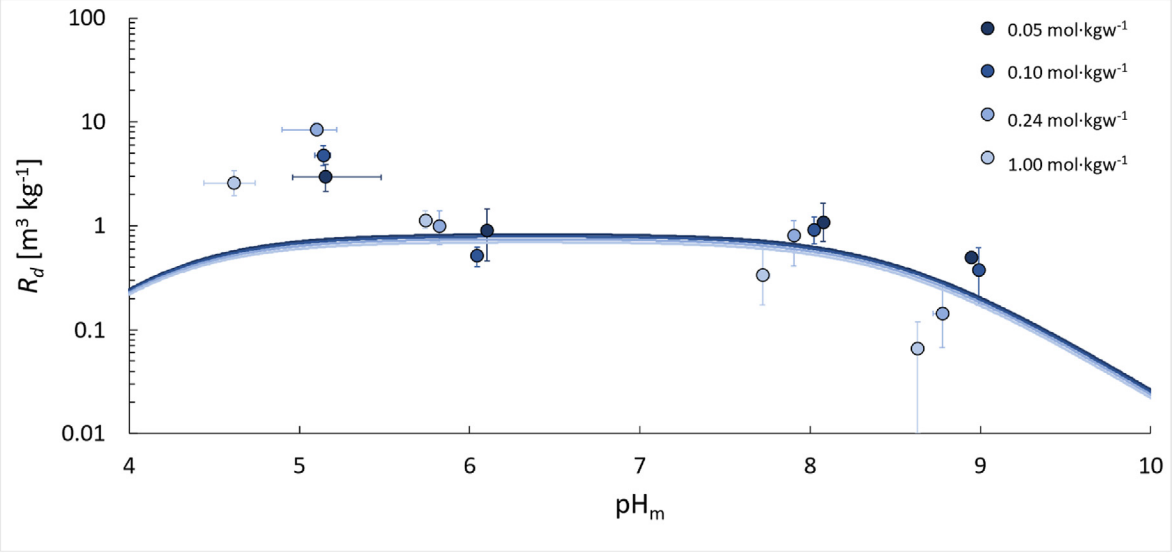

Fig. 2. Se(-II) adsorption onto granite dependencies with respect to Ca–Na–Cl physicochemical solution properties and the resultant surface complexation model.

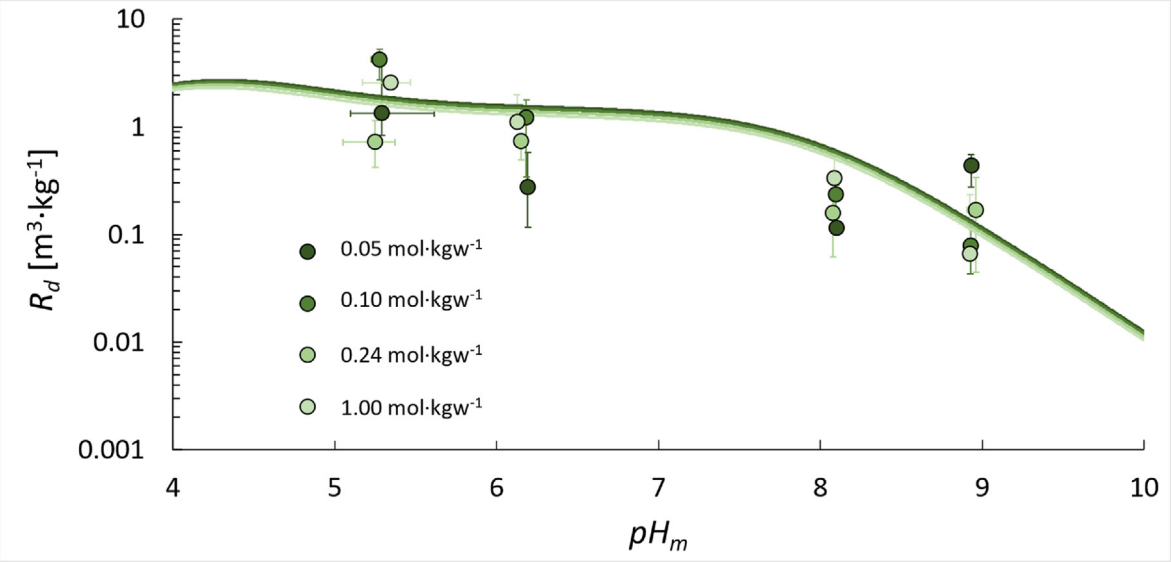

Fig. 3. Se(-II) adsorption onto MX-80 bentonite dependencies with respect to Ca–Na–Cl physicochemical solution properties and the resultant surface complexation model.

Table 9
Surface complexation reactions and optimized surface complexation constants for the simulated surfaces.

Simulated surface	Surface Complexation Reaction	Surface Complexation Constant (Log K)
Granite	≡Feldspar_sOH + HSe^- ↔ ≡Feldspar_sSe^- + H_2O	5.5
	≡Biotite_sOH + HSe^- + H^+ ↔ ≡Biotite_sOH_2HSe	*12.0*
MX-80 Bentonite	≡Albite_sOH + HSe^- ↔ ≡Albite_sSe^- + H_2O	5.5
	≡Montmorillonite_sOH + HSe^- ↔ ≡Montmorillonite_sSe^- + H_2O	*4.5*
	≡Montmorillonite_sOH + HSe^- + H^+ ↔ ≡Montmorillonite_sOH_2HSe	*9.5*

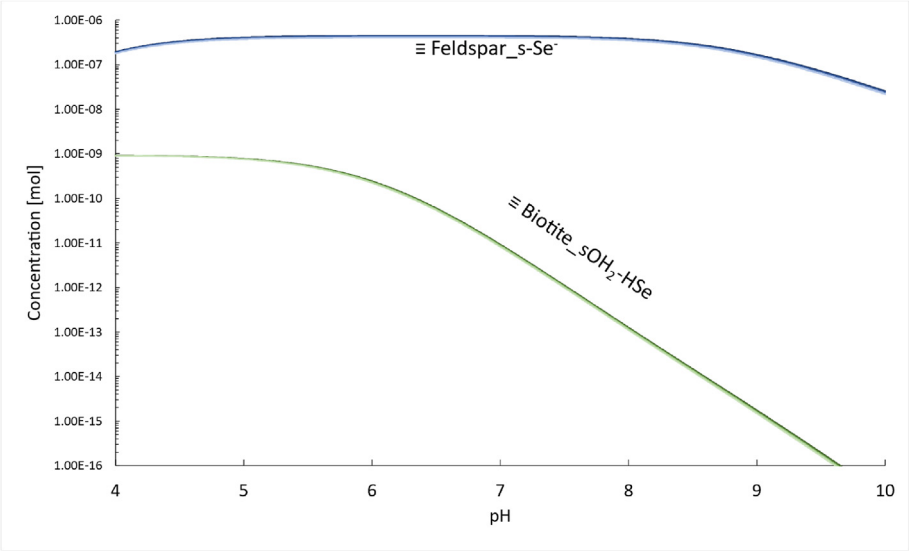

Fig. 4. Expected Se(-II) surface complexation onto the simulated granite surface.

are presumed suitable to describe the decrease in Se(-II) adsorption onto MX-80 bentonite in the 0.1, 0.24, and 1.0 mol•kgw^{-1} Ca–Na–Cl solutions. Regarding Se(-II) adsorption onto MX-80 bentonite in the 0.05 mol•kgw^{-1} Ca–Na–Cl solution, the experimental data presents that R_d at pH_m of 9.0 is within error of the R_d value at pH_m of 6.0. This may allude to a difference in Se(-II) adsorption behaviour with respect to pH_m for only the 0.05 mol•kgw^{-1} Ca–Na–Cl solution. This however does contrast the adsorption behaviour of Se(-II) onto MX-80 bentonite with respect to ionic strength as there is no substantial trend that can be attributed given all data points are within error at any given pH_m value. Therefore, it is currently presumed that Se(-II) adsorption onto MX-80 bentonite in the 0.05 mol•kgw^{-1} Ca–Na–Cl solution would coincide with the adsorption behaviour observed with the

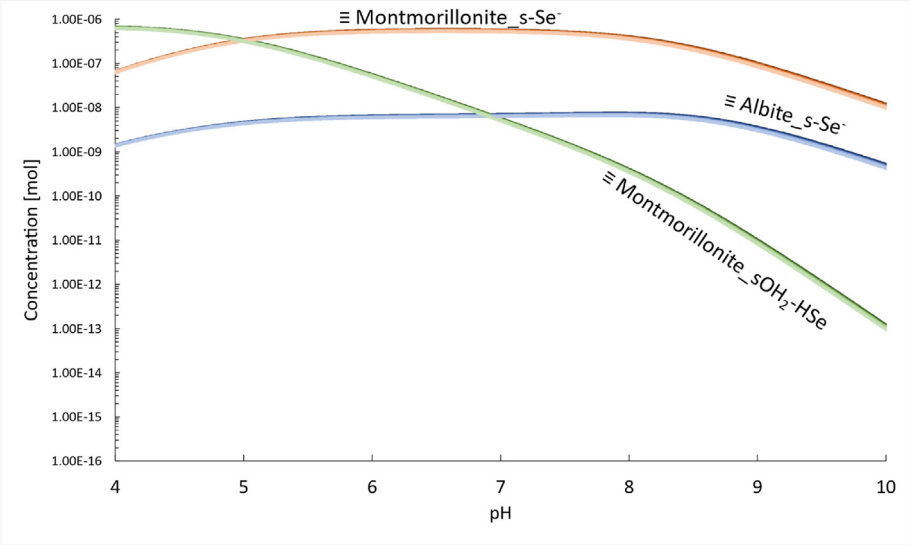

Fig. 5. Expected Se(-II) surface complexation onto the simulated MX-80 bentonite surface.

other solutions. As MX-80 bentonite is assumed to be 85.4% montmorillonite, the adsorption of Se(-II) onto montmorillonite would provide good indication for how MX-80 bentonite would interact with HSe^-. It must be discussed however that Se(-II) adsorption onto pure montmorillonite has presented an ionic strength dependant effect, whereas MX-80 bentonite has not alluded to any ionic strength effects [42,43]. It must be acknowledged that the remaining 14.6% of the MX-80 bentonite which is attributed to quartz, albite, and the amorphous solids may also interact with Se(-II). If any one of these assemblage components display an ionic strength dependency, then there must be a small proportion of MX-80 bentonite which would display ionic strength dependant effects. It may be possible that the heterogenous mixture of mineral assemblages prevents the ionic strength adsorption effect displayed with the homogenous montmorillonite component to be observed as prominently. With no clear evidence that ionic strength effects R_d values, it is not possible to confirm that adsorption of Se(-II) onto MX-80 bentonite is independent of the ionic strength. Two previous studies found that Se(-II) adsorption onto MX-80 bentonite returned R_d values between 1.0 and 5.0 $m^3\ kg^{-1}$ in the neutral pH Na–Ca–Cl solutions, which then decreased to a range of 0.1–1.0 $m^3\ kg^{-1}$ in the more basic pH Na–Ca–Cl solutions [43]. These ranges of R_d values are like the R_d values returned using Ca–Na–Cl solutions from this study. Despite the data being limited, Sugiura et al., determined the adsorption of Se(-II) onto pure montmorillonite returned values that range from 0.1 to 1.0 $m^3\ kg^{-1}$ [42]. These previous studies support the presented results within this study for Se(-II) adsorption onto MX-80 bentonite with R_d values of similar magnitudes.

The adsorption of Se(-II) onto granite and MX-80 bentonite in the CR-10 reference groundwater solution are of interest to the NWMO and their post-closure safety assessment in crystalline rock. These results are beneficial, as this is a representation of how Se(-II) is expected to adsorb in the geosphere with the multitude of ions found in the groundwater. After the 7-day adsorption period for granite, $R_d = (1.8 \pm 0.10)\ m^3 \bullet kg^{-1}$. After the 14-day adsorption period for MX-80 bentonite, $R_d = (0.47 \pm 0.38)\ m^3 \bullet kg^{-1}$. A topic of discussion is that Se(-II) R_d values for granite in CR-10 solution are greater than Se(-II) R_d values for MX-80 bentonite in CR-10. This contrasts what was observed in the Ca–Na–Cl adsorption experiments as granite returned R_d values less than MX-80 bentonite in the same solutions. An explanation for this behaviour is that there may be the formation of an unknown ion pair between Se(-II) and any one of the various background electrolytes found in CR-10 solution which may then adsorb to the surface of granite, but not onto MX-80 bentonite. From Tables 3 and it is apparent that there is an increased amount of mineral assemblage components within granite compared to MX-80 bentonite. It is possible that one of these mineral assemblages is a strong adsorber of the unknown Se(-II) ion pair. Lastly, it has been determined that Se(-II) adsorption onto granite is dependant upon the ionic strength with R_d decreasing as ionic strength increases. The returned R_d value for Se(-II) adsorption onto granite in CR-10 solution is greater than any R_d value in Ca–Na–Cl solutions, except at $pH_m = 5.0$. When considering the ionic strength of the CR-10 solution is approximately 0.24 $mol \bullet kgw^{-1}$, the large R_d value suggests that the ionic strength dependency effects may be dominated by the adsorption of the unknown aqueous Se(-II) species, secondary redox processes, or possible precipitation of a crystalline Se compound. Some possible examples of alkali metal selenides to consider based upon the ions present in CR-10 include $Li_2Se(cr)$, $Na_2Se(cr)$, $NaHSe(aq)$, $K_2Se(cr)$, $CaSe(cr)$, and $SrSe(cr)$ [45]. It must be briefly mentioned that the increased R_d determined from Se(-II) adsorption onto granite in CR-10 solution compared to in Ca–Na–Cl solutions, is a benefit to the NWMO in their post-closure safety assessment. An example is if there is an alkali metal selenide forming in the groundwater representation used within these experiments, it is presumed that the same alkali metal selenide will form in the groundwater present within the DGR. This would decrease the aqueous concentration of Se(-II) present within the geosphere, if Se(-II) were to exist in the geosphere in a mobile form, thus decreasing the mobility associated with Se(-II).

With an effort being made internationally by other countries seeking to successfully implement their own DGR, there must be adequate research carried out specific to Se(-II) migration within other geological environments. These studies are beneficial to the NWMO as it allows for a comparison of accepted Se(-II) R_d values that are being utilized to prove the different nuclear agencies post-closure safety assessments. In the past there have been reports that the adsorption of Se(-II) for usage in the Swiss or Finnish waste disposal programs. Despite the differences in the bedrock, and groundwater chemistry observed between different international

DGR projects, the adsorption of Se(-II) is consistently characterized by low adsorption, as R_d values range from undetermined values to approximately 0.03 m^3 kg^{-1} [79,80]. The low amount of Se(-II) adsorption is also observed within this study despite the adsorbent materials being granite and MX-80 bentonite. It further has been reported that Se(-II) adsorption onto sedimentary rocks in Na–Ca–Cl solution does not exceed 5.00 m^3 kg^{-1} [43,81]. The increased adsorption within the Canadian geological environment is possibly attributed to the increased solution ionic strength. This comparison is still considered to provide confidence in the presented R_d values for Se(-II) adsorption onto both granite and MX-80 bentonite, as the R_d values are within the expected range of approximately 1.00×10^{-2} m^3 kg^{-1} to 1.00×10^{1} m^3 kg^{-1} at the similar neutral to basic pH regimes previously studied.

A current presumption is that in the batch adsorption experiments involving Ca–Na–Cl solutions that were specifically at $pH_m = 5.0$, the increased adsorption is possibly the result of the increased electrostatic interactions that have been discussed previously. There is also the possibility that Se precipitate formed within the polycarbonate reaction vessel during the experiment, which would have an influence of increasing the R_d value. In Fig. S1 there are some data presented which exhibit Eh vs. pH_m characteristics that should indicate this precipitation did occur. Throughout the experiment there was no visible precipitate that was formed within solution, and as the initial Se(-II) concentration was defined to be below the known Se(-II) solubility limit, it was still believed no precipitate formed. In previous Se(-II) adsorption experiments an ultrafiltration step was carried out, and it is believed this would remove any precipitate, had it formed in solution [40–42]. It is the recommendation of the authors that all future Se(-II) adsorption experiments utilize an ultrafiltration step to prevent this issue.

Upon completion of experiments, surface complexation modelling was performed to simulate the adsorption of Se(-II) onto granite and MX-80 bentonite. These models have been optimized using data obtained from batch adsorption experiments. R_d was calculated though a summation of adsorption of Se(-II) onto each assemblage component then divided by the total Se(-II) concentration.

$$R_d = \sum_i \frac{[Se(-II)\ adsorbed\ onto\ (mineral\ assemblage)_i]}{[Se(-II)]_{Total}} \quad (5b)$$

As a reminder, the simulated granite surface was assumed to be 56.0% K-Feldspar, 34.0% quartz, and 3.0% biotite while the simulated MX-80 bentonite surface was assumed to be 85.4% montmorillonite, 3.62% quartz, and 3.54% albite. It must be stated that a goal of this modelling approach is to be able to define surface complexation reactions using mineral assemblages, which may be used within all surfaces to be modelled, if that mineral assemblage is present. This model will take into consideration any experimental proof about adsorption of Se(-II) onto individual mineral surfaces, or if required, proof about adsorption of Se(-II) onto silanol, aluminol, and ferrol surface sites to propose surface complexation reactions. An assumption is that if adsorption of an element is possible on one mineral assemblage within a given heterogenous mineral, then adsorption onto the identical mineral assemblage in a different heterogenous mineral would differ only based on the different proportion considered within each surface, and not the interaction between the element and surface being simulated. This is therefore considered to imply that the surface complexation constant be the same for a given surface complexation reaction with an assemblage mineral that is used in any heterogenous surface model. The surface complexation models that simulate the adsorption of Se(-II) onto granite and MX-80 bentonite are successful and give possible insight into the dominant adsorbing minerals and their adsorption mechanisms.

Of the mineral assemblage components considered, quartz was not presumed needed to have any surface complexation reactions modelled as Se(-II) adsorption onto quartz has previously returned low or undetermined R_d values [40]. An assumption about quartz is that it is contains only silanol surface sites which have a point of zero charge (PZC) of 2.2. This is considered, as it is known that a low PZC would have an effect of repelling anions away from the surface as the silanol sites become more negatively charged in neutral-alkaline systems [40]. Which would lead to a decrease in Se(-II) adsorption onto quartz, if any were to occur. Therefore, the low experimental R_d values, the highly crystalline structure, and the low PZC are presumed justification for not including any Se(-II) – quartz surface complexation reactions within either the granite or MX-80 bentonite surface complexation models.

Biotite is a phyllosilicate mineral that has been shown to be a dominant adsorber of Se(-II) and as such a surface complexation reaction with biotite was considered necessary. Justification for the existence of the non-specific Se(-II) surface complex with biotite comes from a previous study that utilized only an outer-sphere complex within a triple layer surface complexation model and found success in simulating Se(-II) adsorption onto biotite [40]. Biotite was shown to return an R_d value of similar magnitude to the R_d determined using granite [40]. An aspect to consider about the biotite component within the granite model is that it only accounts for 3.0% of the total granite surface. Then taking into consideration the similar R_d values being found for biotite and granite with respect to Se(-II) adsorption, it is predicted that biotite must be a dominant Se(-II) adsorbing mineral within granite. Biotite may play a more important role than this model can describe as iron oxides play an important role in the adsorption of selenites within granite, and they will form when biotite is weathered [40,82]. Despite this possible secondary process, the presentation of a $\equiv Bioite\_sOH_2HSe$ surface complex is believed justified.

The remaining mineral assemblage considered within the granite surface is the feldspar component which is assumed to comprise 56.0% of granite. It is anticipated this may be a dominant adsorber purely based on the proportion within granite. One important consideration is that tectosilicates in general do not display much adsorption as there is approximately only 10.0% Se(-II) adsorption onto tectosilicates at any pH [40]. This would require the biotite component of the model to be able to provide up to 90.0% possibly of the remaining Se(-II) adsorption. This may be possible as Se(-II) adsorption onto phyllosilicates show pH dependency trends with Se(-II) adsorption decreasing from approximately 80.0% at pH = 8.5 to approximately 6.0% at pH = 12.0 [40]. It is therefore presumed that it may be possible for there to be a possible 90.0% Se(-II) adsorption onto biotite when accounting for variations in mineral assemblage proportions, or redox process that led to adsorption. With the justification to continue using feldspar as a possible Se(-II) adsorber, both possible surface complexation reactions were considered. However, it was not possible to discern exact Se(-II) adsorption mechanisms onto feldspar from existing literature. As such, with knowledge that feldspar is comprised of silanol and aluminol surface sites it may be possible to justify one or both surface complexation reactions. As previously mentioned, the adsorption of Se(-II) is similar to Se(IV) but not Se(VI), which is beneficial as there is evidence that Se(IV) adsorbs onto aluminol sites. This is presumed to justify the inclusion of a feldspar surface complexation reaction. Previously, Peak et al., were able to characterize the formation of Se(IV) – aluminol inner-sphere surface complexes using XAS measurements [24]. Of the two surface complexes, one was determined to be bidentate, while the other was a monodentate surface complex. Based upon the fact Se(IV)

forms as an oxyanion which would have a larger molecular size compared to Se(-II), it may not be possible for Se(-II) to form as a bidentate surface complex if the aluminol surface sites are too distant. Based upon this assumption, only the ≡*Feldspar_sSe*$^-$ surface complex has been considered. As previously mentioned, the feldspar surface within granite, and the albite surface within MX-80 bentonite are both defined using the same protolysis constants, and site density. These surfaces are simulated identically with the only differences being the SSA within the model, and the naming convention. Using the same reasons for the justified inclusion of a Se(-II) −feldspar surface complex, there has been a ≡*Albite_sSe*$^-$ surface complex proposed within the MX-80 bentonite simulation.

From a previous surface complexation modelling approach presented by Walker et al., it was found possible to model the adsorption of Se(-II) onto MX-80 bentonite surface using a montmorillonite surface, and the two different forms of the Se(-II) surface complexation reactions within the well known 2SPNE SC model [43]. Additionally, Sugiura et al., performed a systematic study investigating Se(-II) adsorption onto montmorillonite and as mentioned previously, Se(IV) and Se(-II) show similar adsorption behaviour thus it would be expected that Se(-II) would adsorb onto the aluminol sites within MX-80 bentonite. With montmorillonite being a known phyllosilicate mineral that contains a single alumina octahedral sheet sandwiched between two silica tetrahedral sheets, it is presumed that there could exist a ≡*Montmorillonite_sSe*$^-$ surface complex. This does not dismiss the possibility of ≡*Montmorillonite_sOH$_2$HSe* surface complex, however. Therefore, this was reason to further consider both surface complexation reactions for Se(-II) and montmorillonite.

It is important to recognize the potential Se(-II) has displayed for adsorption through a secondary redox process with the surface. These reactions will play a role in the adsorption of Se(-II) onto both adsorbents which may contribute to the proposed surface complexation or may account for discrepancies between the modelling and experimental data. There is belief that one of the most effective methods of Se(-II) adsorption is through a redox reaction involving Fe(III) [42]. One known characteristic of montmorillonite is the capability it displays for allowing isomorphic substitutions of Al with Fe at the edges of the octahedral sheet [83]. As a result, any Se(-II) that would adsorb onto a ferrol site that is within biotite or montmorillonite, would be oxidized to Se(0) and contribute to larger R_d values. There has been proof for this redox reaction from XAS results determined by Sugiera et al. [34]. This secondary redox process may also account for the difference displayed at $pH_m = 5.0$ in Fig. 2. Despite the possibility of this redox process, the presented surface complexation models are successful simulations of Se(-II) adsorption behaviour. From the modelling results, it appears that it is possible to simulate Se(-II) adsorption onto granite using the feldspar and biotite component, while MX-80 bentonite requires albite and montmorillonite components.

At the present, it is presumed that this study presents the hypothesized ≡*Feldspar_sSe*$^-$ surface complex for the first time, while a previous study utilized the ≡*Bioite_sOH$_2$HSe* surface complex [40]. Future work will investigate the capacity to improve the surface complexation modelling results with respect to the granite simulations. There is a good fit observed when comparing Se(-II) adsorption onto MX-80 bentonite R_d values to the simulation results that are shown in Fig. 3. In the past, a previous MX-80 bentonite surface complexation model presented by Walker et al., required both ≡*Montmorillonite_sSe*$^-$ and ≡*Montmorillonite_sOH$_2$HSe* surface complexes to successfully simulate Se(-II) adsorption onto MX-80 bentonite [43]. This model is presently considered to build upon this previous model through addition of a new hypothesized ≡*Albite_sSe*$^-$ surface complex which is based upon the granite model including the new ≡*Feldspar_sSe*$^-$ surface complex. Fig. S2 has been included in the supplementary material and depicts a comparison of the simulation results that have been presented in Fig. 3, with a simulation that contains no albite surface complex. Though at the present there is an insignificant difference in the simulation results. The albite component within MX-80 bentonite is presently considered to comprise 3.54%, so the significance of Se(-II) adsorption onto albite from the simulations could be insignificant as well.

6. Conclusion

The adsorption behaviour of Se(-II) onto granite and MX-80 bentonite has been studied in Ca–Na–Cl and CR-10 solutions. Adsorption kinetic experiments using 0.05 and 1.0 mol•kgw^{-1} Ca–Na–Cl solutions show that Se(-II) adsorption reaches steady-state conditions before 7 days and 14 days for granite and MX-80 bentonite, respectively. An investigation was then performed that elucidated the influence that Ca–Na–Cl physicochemical solution properties have on Se(-II) adsorption behaviour. Granite and MX-80 bentonite display opposing trends with respect to ionic strength dependent effects as R_d decreases for granite with an increase in solution ionic strength, while MX-80 bentonite shows no change in R_d. Both adsorbents do display adsorption behaviour typically associated with anions, providing confidence that Se(-II) was the dominant Se redox state throughout experiments. A final Se(-II) adsorption experiment was carried out in CR-10 groundwater representative solution, and the R_d value associated with granite is (1.80 ± 0.10) m^3•kg^{-1} whereas MX-80 bentonite is (0.47 ± 0.38) m^3•kg^{-1}. These Se(-II) R_d values are on par with previously published Se(-II) R_d values used by other international nuclear disposal programs providing confidence in these reported values. Batch adsorption experiment data was subsequently used to optimize surface complexation constants for two different component additive surface complexation models that use mineral assemblages to simulate granite and MX-80 bentonite surfaces. Granite was simulated using feldspar, quartz, and biotite. Whereas MX-80 bentonite was simulated with montmorillonite, quartz, and albite. Se(-II) adsorption onto granite was best simulated with Se(-II) specifically adsorbing to feldspar (≡Feldspar_sSe$^-$), and Se(-II) adsorbing non-specifically to biotite (≡Biotite_sOH$_2$HSe). MX-80 bentonite utilized a non-specific Se(-II) adsorption reaction onto albite (≡Albite_sSe$^-$), in conjunction with montmorillonite capable of adsorbing both specifically (≡Montmorillonite_sSe$^-$), and non-specifically (≡Montmorillonite_sOH$_2$HSe). These experimental results and surface complexation models that have been presented in this work are beneficial as they can help further the scientific understanding of Se(-II) adsorption and adsorption mechanisms.

Declaration of competing interest

The authors declare that they have no known competing financial interests or personal relationships that could have appeared to influence the work reported in this paper.

Acknowledgements

This work was funded by the Nuclear Waste Management Organization.

Appendix A. Supplementary data

Supplementary data to this article can be found online at https://doi.org/10.1016/j.net.2023.06.049.

References

[1] P. Gierszewski, A. Parmenter, Confidence in Safety – South Bruce Site, Nuclear Waste Management Organization, 2022. NWMO-TR-2022-15.
[2] P. Gierszewski, A. Parmenter, Confidence in Safety – Revell Site, Nuclear Waste Management Organization, 2022. NWMO-TR-2022-14.
[3] Postclosure Safety Assessment of a Used Fuel Repository in Crystalline Rock, Nuclear Waste Management Organization, 2017. NWMO-TR-2017-02.
[4] N. Naserifard, A. Lee, K. Birch, A. Chiu, X. Zhang, Deep Geological Repository Conceptual Design Report Crystalline/Sedimentary Rock, Nuclear Waste Management Organization, 2021. APM-REP-00440-0211-R000.
[5] G. Jörg, R. Bühnemann, S. Hollas, N. Kivel, K. Kossert, S. Van Winckel, G. Lierse v Gostomski, Preparation of radiochemically pure ^{79}Se and highly precise determination of its half-life, Appl. Radiat. Isot. 63 (2010) 2339–2351.
[6] N. Jordan, C. Franzen, J. Lutzenkirchen, H. Foerstendorf, D. Hering, S. Weiss, K. Heim, V. Brendler, Adsorption of selenium(VI) onto nano transition alumina, Environ. Sci. Nanotech. (2018).
[7] N. Jordan, A. Ritter, H. Foerstendorf, A.C. Scheinost, S. Weiss, K. Heim, J. Grenzer, A. Mucklich, H. Reuther, Adsorption mechanism of selenium(VI) onto maghemite, Geochem. Cosmochim. Acta 103 (2013) 63–75.
[8] X. Li, E. Puhakka, J. Ikonen, M. Soderland, A. Lindberg, S. Holgersson, A. Martin, M. Siitari-Kauppi, Sorption of Se species on mineral surfaces, part 1: batch sorption and multi-site modelling, Appl. Geochem. 95 (2018) 147–157.
[9] W.A. Hardy, G. Silvey, C.H. Townes, B.F. Burke, M.W.P. Strandberg, G.W. Parker, V.W. Cohen, The nuclear moments of ^{79}Se, Phys. Rev. 6 (1953) 1532–1537.
[10] K. Videnska, S. Palagyi, K. Stamberg, H. Vodickova, V. Havlova, Effect of grain size on the sorption and desorption of SeO_4^{2-} and SeO_3^{2-} in columns of crushed granite and fracture infill from granitic water under dynamic conditions, J. Radioanal. Nucl. Chem. 298 (2013) 547–554.
[11] B. Bar-Yosef, D. Meek, Selenium sorption by kaolinite and montmorillonite, Soil Sci. 144 (1987) 11–19.
[12] M. Gupta, S. Gupta, An overview of selenium uptake, metabolism, and toxicity in plants, Front. Plant Sci. 7 (2017) 2074.
[13] Y. Zhang, J. N. Moore, Selenium fractionation and speciation in a wetland system, Environ. Sci. Technol. 30 (20XX) 2613-2619.
[14] H. Koch-Steindl, G. Prohl, Consideration on the behaviour of long-lived radionuclides in the soil, Radiat. Environ. Biophys. 40 (2001) 93–104.
[15] C. Medri, G. Bird, Non-Human Biota Dose Assessment Equations and Data, Nuclear Waste Management Organization, 2015. NWMO-TR-2014-02 R001.
[16] M. Greger, Uptake of Nuclides on Plants, Svensk Karnbranslehantering AB (SKB), 20014, TR-04-14.
[17] M. Ho, The Long-Term Biogeochemistry of ^{79}Se, ^{99}Tc, and ^{90}Sr in Complex Environmental Systems, PhD Thesis, Department of Chemistry – Radiochemistry, University of Helsinki, 2022.
[18] J. J. J. Racette, S. Nagasaki, Pursuing Long-Term Nuclear Waste Safety in Canada for Seven Generations and beyond: A Radio-Ethnobotany Case Study in: 41st Annual Conference of the Canadian Nuclear Society and 46th Annual CNS/CNA Student Conference June 5 – 8 2022.
[19] S. Das, J.M. Hendry, J. Essilfie-Dughan, Adsorption of selenate onto ferrihydrite, geothite, and lepidocrocite under neutral pH conditions, Appl. Geochem. 28 (2013) 185–193.
[20] S. Goldberg, Macroscopic experimental and modelling evaluation of selenite and selenate adsorption mechanisms on gibbsite, Soil Sci. Soc. Am. J. 78 (2013) 473–479.
[21] N. Mayordomo, H. Foerstendorf, J. Lutzenkirchen, K. Heim, S. Weiss, U. Alonso, T. Missana, K. Schmeide, N. Jordan, Selenium(IV) sorption onto γ-Al_2O_3: a consistent description of the surface speciation by spectroscopy and thermodynamic modelling, Environ. Sci. Technol. 52 (2018) 581–588.
[22] H.K. Hami, R.F. Abbas, E.M. Eltayef, N.I. Mahdi, Applications of aluminum oxide and nano aluminum oxide as adsorbents: review, Samarra J. Pure Appl Sci. 2 (2020) 19–32.
[23] U.K. Saha, C. Liu, L.M. Kozak, P.M. Huang, Kinetics of selenite adsorption on hydroxyaluminum and hydroxyaluminosilicate-montmorillonite complexes, Soil Sci. Soc. Am. J. 68 (2004) 1197–1209.
[24] D. Peak, Adsorption mechanisms of selenium oxyanions at the aluminum oxide/water interface, J. Colloid Interface Sci. 303 (2006) 337–345.
[25] W.-H. Kuan, S.-L. Lo, M.K. Wang, C.-F. Lin, Removal of Se(IV) and Se(VI) from water by aluminum oxide coated sand, Wat. Res. 32 (1998) 915–923.
[26] Y.L. Jan, T.H. Wang, M.H. Li, S.C. Tsai, Y.Y. Wei, C.N. Hsu, S.P. Teng, Evaluating adsorption ability of granite to radioselenium by chemical sequential extraction, J. Radioanal. Nucl. Chem. 273 (2007) 299–306.
[27] K. Videnska, V. Havlova, Retention of anionic species on granite: influence of granite composition – 12129 in: WM2012 conference, pheonix, Arizona, USA, in: WM2012 Conference, February 26 - March 1, 2012. February 26-March 1, 2012, Pheonix, Arizona, USA.
[28] F. Seby, M. Potin-Gautier, E. Giffaut, G. Borge, O.F. X Donard, A critical review of thermodynamic data for selenium species at 25°C, Chem. Geol. 171 (2001) 173–194.
[29] M. Fujita, M. Ike, R. Hashimoto, T. Nakagawa, K. Yamaguchi, S.O. Soda, Characterizing kinetics of transport and transformation in water-sediment microcosm free from selenium contamination using a simple mathematical model, Chemosphere 58 (2005) 705–714.
[30] F. Chen, P.C. Burns, R.C. Ewing, *^{79}Se: geochemical and crystallo-chemical retardation mechanisms*, J. Nucl. Matls. 275 (1999) 81–94.
[31] I. Zafeiriou, D. Gasparatos, I. Massas, Adsorption/Desorption patterns of selenium for acid and alkaline soils of xerothermic environments, Environments 7 (2020).
[32] J.S. Yamani, A.W. Lounsbury, J.B. Zimmerman, Adsorption of selenite and selenate by nanocrystalline aluminum oxide, neat and impregnated chitosan beads, J. of Water Research 50 (2014) 373–381.
[33] Y. Legoux, G. Blain, R. Guillaumont, G. Ouzounian, L. Brillard, M. Hussonnois, K_d measurements of activation, fission, and heavy elements in water/solid phase systems, Radiochim. Acta 58/59 (1992) 211–218.
[34] M.-H. Baik, S.-Y. Lee, J. Jeong, Sorption and reduction of selenite on chlorite surfaces in the presence of Fe(II) ions, J. Environ. Radioact. 126 (2013) 209–215.
[35] T. Missana, U. Alonso, M. Garcia-Gutierrez, Experimental Study and modelling of selenite sorption onto illite and smectite clays, J. Colloid Interface Sci. 334 (2009) 132–138.
[36] K. Piekkari, K. Ohenoja, V. Isteri, P. Tanskanen, M. Illikainen, Immobilization of heavy metals, selenate, and sulphate from a hazardous industrial side stream by using calcium sulfoaluminate-belite cement, J. Clean. Prod. 258 (2020), 120560.
[37] C.E. Cowan, J.M. Zachara, C.T. Resch, Solution ion effects on the surface exchange of selenite on calcite, Geochem. Cosmochim. Acta 54 (1990) 2223–2234.
[38] S. Goldberg, R.A. Glaubig, Anion sorption on a calcerous, montmorillonite soil-selenium, Soil Sci. Soc. Am. J. 52 (1988) 954–988.
[39] K.V. Ticknor, T.T. Vandergraaf, J. McMurray, L. Biosvenue, D.L. Wilkin, Parametric Studies of Factors Affecting Se and Sn Sorption, Atomic Energy of Canada Ltd., 1996. AECL TR-723, COG-95-554.
[40] Y. Iida, T. Yamaguchi, T. Tanaka, Sorption Behaviour of hydroselenide (HSe^-) onto iron containing minerals, J. Nucl. Sci. Technol. 51 (2014) 305–322.
[41] Y. Iida, T. Tanaka, T. Yamaguchi, S. Nakayama, Sorption behaviour of selenium(-II) on rocks under reducing conditions, J. Nucl. Sci. Technol. 48 (2011) 279–291.
[42] Y. Sugiura, Tomura, T. Ishidera, R. Doi, P. Clarence, M. Francisco, H. Shiwaku, T. Kobayashi, D. Matsumura, Y. Takahashi, Y. Tachi, Sorption behaviour of selenide on montmorillonite, J. Radioanal. Nucl. Chem. 324 (2020) 615–622, 43, 59, 66-72.
[43] A. Walker, J. Racette, T. Saito, T.T. Yang, S. Nagasaki, Sorption of Se(-II) on illite, MX-80 bentonite, shale, and limestone in Na-Ca-Cl Solutions, Nucl. Eng. Technol. 54 (2022) 1616–1622.
[44] F.P. Bertetti, Determination of Sorption Properties for Sedimentary Rocks under Saline, Reducing, Conditions – Key Radionuclides, Nuclear Waste Management Organization, 2016. NWMO-TR-2016-08.
[45] A. Olin, B. Nolang, E.G. Osadchii, L.-O. Ohman, E. Rosen, Chemical Thermodynamics of Selenium, Nuclear Energy Agency, 2004.
[46] S. Nagasaki, T. Saito, T.T. Yang, Sorption Behaviour of Np(V) on illite, shale, and MX-80 in high ionic strength solutions, J. Radioanal. Nucl. Chem. 308 (2016) 143–153.
[47] M. Altmaier, V. Neck, T. Fanghanel, Solubility of Zr(IV), Th(IV), and Pu(IV) hydrous oxides in $CaCl_2$ solutions and the formation of ternary Ca-M(IV)-OH complexes, Radiochim. Acta 96 (2008) 541–550.
[48] M. Altmaier, V. Metz, V. Neck, R. Muller, T. Fanghanel, Solid-Liquid equilibria of $Mg(OH)_2$(cr) and $Mg_2(OH)_3Cl{\bullet}4H_2O$(cr) in the system Mg-Na-H-OH-Cl-H_2O at 25°C, Geochem. Cosmochim. Acta 67 (2003) 3595–3601.
[49] J. Zhao, H. Matsune, S. Takanaka, N. Kishida, Reduction of selenate with hydrazine monohydrate over Pt crystals in aqueous solution, Chem. Eng. J. 308 (2017) 963–973.
[50] J.P. Chen, L.L. Lim, Key factors in chemical reduction by hydrazine for recovery of precious metals, Chemosphere 49 (2002) 363–370.
[51] Y. Iida, T. Yamaguchi, S. Nakayama, T. Nakajima, Y. Sakamoto, The solubility of metallic selenium under anoxic conditions, Mater. Res. Soc. Symp. Proc. 663 (2001).
[52] Y. Iida, T. Tanaka, T. Yamaguchi, S. Nakayama, Solubility of selenium at high ionic strength under anoxic conditions, J. Nucl. Sci. Technol. 47 (2010) 431–438.
[53] Y. Iida, T. Yamaguchi, T. Tanaka, A. Kitamura, S. Nakayama, Determination of the Solubility Limiting Solid of Selenium in the Presence of Iron under Anoxic Conditions, Japanese Atomic Energy Research Institute, 2010.
[54] Y. Iida, T. Tanaka, T. Yamaguchi, S. Nakayama, Solubility of selenium at high ionic strength under anoxic conditions, J. Nucl. Sci. Technol. 47 (2010) 431–438.
[55] T.T. Yang, Personal Correspondence, Nuclear Waste Management Organization, 2018.
[56] T.T. Yang, Personal Correspondence, Nuclear Waste Management Organization, 2023.
[57] M.H. Bradbury, B. Baeyens, Physico-Chemical Characterisation Data and Sorption Measurements of Cs, Ni, Eu, Th, U, Cl, I, and Se on MX-80 Bentonite, Paul Schrerrer Institut, 2011. PSI Bericht Nr. 11-05.
[58] D. Dixon, A. Mam, S. Rimal, J. Stone, G. Siemens, Bentonite Seal Properties in Saline Water, Nuclear Waste Management Organization, 2018. NWMO-TR-2018-20.
[59] S. Nagasaki, Sorption Properties of Np on Shale, Illite, and Bentonite under Saline, Oxidizing, and Reducing Conditions, Nuclear Waste Management Organization, 2018. NWMO-TR-2018-02.
[60] J. Goguen, A. Walker, J. Racette, J. Riddoch, S. Nagasaki, Sorption of Pd on illite, MX-80 bentonite, shale in Na-Ca-Cl solutions, Nucl. Eng. Technol. 53 (2021)

894–900.
[61] D.L. Parkhurst, C.A.J. Appelo, Description of input and examples for PHREEQC version 3 – a computer program for speciation, batch-reaction, one-dimensional transport, and inverse geochemical calculations, U.S. Geological Survey Techniques and Methods (2013).
[62] R. Doi, A. Kitamura, M. Yui, JAEA Thermodynamic Database for Performance Assessment of Geological Disposal of High-Level and TRU Wasters: Selection of Thermodynamic Data of Selenium, Japanese Atomic Energy Agency, 2009. JAEA-Review 2009-051.
[63] S. Licht, F. Forouzan, Speciation analysis of aqueous polyselenide solutions, J. Electrochem. Soc. 142 (1995) 1546–1551.
[64] L.E. Lyons, T.L. Young, Alkaline selenide, polyselenide electrolytes: concentrations, absorption spectra, and formal potentials, Aust. J. Chem. 39 (1986) 511–527.
[65] E. Yalcintas, X. Gaona, M. Altmaier, K. Dardenna, R. Polly, H. Geckeis, Thermodynamic description of Tc(IV) solubility and hydrolysis in dilute to concentrated NaCl, $MgCl_2$ and $CaCl_2$ solutions, Dalton Trans. 45 (2016) 8916–8936.
[66] M.H. Bradbury, B. Baeyens, A mechanistic description of Ni and Zn sorption on Na-montmorillonite Part I: titration and Sorption Measurements, J. Contam. Hydrol. 27 (1997) 199–222.
[67] M.H. Bradbury, B. Baeyens, A mechanistic description of Ni and Zn sorption on Na-montmorillonite Part II: modelling, J. Contam. Hydrol. 27 (1997) 223–248.
[68] M.H. Bradbury, B. Baeyens, A Quantitative Mechanistic Description of Ni, Xn, and Ca Sorption on Na-Montmorillonite, Paul Schreer Institute, 1995. PSI Bericht Nr. 95-12.
[69] M.H. Bradbury, B. Baeyens, Sorption modelling on illite Part 1: titration measurements and sorption of Ni(II), Co(II), Eu(III), and Sn(IV), Geochem. Cosmochim. Acta 73 (2009) 990–1003.
[70] M.H. Bradbury, B. Baeyens, Sorption modelling on Illite Part 2: actinide sorption and linear free-energy relationships, Geochem. Cosmochim. Acta 73 (2009) 1004–1013.
[71] B. Grambow, M. Fattahi, G. Montavon, C. Moisan, E. Giffaut, Sorption of Cs, Ni, Pb, Eu(III), Am(III), Cm, Ac(III), Tc(IV), Th, Zr, and U(IV) on MX-80 bentonite: an experimental approach to assess model uncertainty, Radiochim. Acta 94 (2006) 627–636.
[72] X. Li, A. Puhakka, L. Liu, W. Zhang, J. Ikonen, A. Lindberg, M. Slitari-Kauppi, Multi-site surface complexation modelling of Se(IV) sorption on biotite, Chem. Geol. 533 (2020), 119433.
[73] C. Tournassat, A. Neaman, F. Villieras, D. Bosbach, L. Charlet, Nanomorphology of montmorillonite particles: estimation of the clay edge sorption site density by low-pressure gas adsorption and AFM observations, Am. Mineral. 88 (2003) 1989–1995.
[74] C.H. Wu, S.L. Lo, C.F. Lin, C.Y. Kuo, Modelling competitive adsorption of molybdate, sulfate, and selenate on γ-Al_2O_3 by the triple layer model, J. Colloid Interface Sci. 233 (2001) 259–264.
[75] Y. Iida, T. Yamaguchi, T. Tanaka, K. Hemmi, Sorption Behaviour of thorium onto granite and its constituent minerals, J. Nucl. Sci. Technol. 53 (2016) 1573–1584.
[76] H. Wanner, Y. Albinsson, O. Karnland, E. Wieland, P. Wersin, L. Charlet, The acid/base chemistry of montmorillonite, Radiochim. Acta 66/67 (1994) 157–162.
[77] S.V. Mattigod, A.S. Gibali, A.L. Page, Effect of ionic strength and ion pair formation on the adsorption of nickel onto kaolinite, Clay Clay Miner. 27 (1976) 411–416.
[78] K.V. Ticknor, J. McMurray, A study of selenium and tin sorption on granite and geothite, Radiochim. Acta 73 (1996) 149–156.
[79] B. Baeyens, T. Thoenen, B.H. Bradbury, M. Marques-Fernandes, Sorption data bases for argillaceous rocks and bentonite for the provisional safety analyses for SGT-E2, Nat. Coop. for the Dispos. Of Radioactive Waste (2014). NAGRA TR 12-04.
[80] M. Soderlund, M. Lusa, S. Virtanen, I. Valimaa, M. Hakanen, J. Lehto, Distribution Coefficients of Caesium, Chlorine, Iodine, Niobium, Selenium, and Technetium on Olkiluoto Soils, Posiva, 2014. Working Report 2013-068.
[81] P. Vilks, T. Yang, Sorption of Selected Radionuclides on Sedimentary Rocks in Saline Conditions – Updated Sorption Values, Nuclear Waste Management Organization, 2018 NWMO-TR-2018-03.
[82] C.R. Twidale, J.A. Bourne, J.R. Vidal Romani, Origin of miniature mogotes in granite, king rocks, southern yilgarn block, western Australia, Cuaternario Geomorfol. 13 (1999) 33–34.
[83] C. Tournassat, J.-M. Greneche, D. Tisserand, L. Charlet, The titration of clay minerals 1. Discontinuous backtitration combined with CEC measurements, J. Colloid Interface Sci. 273 (2004) 224–233.